Pergamon

PII S1359-6454(96)00145-0

Acta mater. Vol. 45, No. 1, pp. 157–175, 1997

1359-6454/97 $17.00 + 0.00

SHOCK-INDUCED DEFORMATION TWINNING IN TANTALUM

L. E. MURR[1]†, M. A. MEYERS[2], C.-S. NIOU[1], Y. J. CHEN[2], S. PAPPU[1] and C. KENNEDY[1]

[1]Department of Metallurgical and Materials Engineering, The University of Texas at El Paso, El Paso, TX 79968, U.S.A. and [2]Department of Applied Mechanics and Engineering Sciences, University of California, San Diego, La Jolla, CA 92093, U.S.A.

(Received 8 December 1995; accepted 19 April 1996)

Abstract—Shock-wave deformation of tantalum to a pressure of 45 GPa and duration of 1.8 μs generates profuse twinning. The post-shock mechanical response is significantly affected, with shock hardening exceeding the expected hardening due to the transient shock strain $\epsilon_s = (4/3)\ln(V/V_0)$; this enhanced hardening, and other alterations in response, are attributed to the barriers presented to plastic deformation by the deformation twins.

A constitutive model is proposed that predicts the threshold shock stress for mechanical twinning; it is based on the application of the Swegle–Grady relationship between shock stress and strain rate to constitutive equations describing the critical stress for slip and twinning. This constitutive model incorporates grain-size effects and predicts a threshold twinning stress that is a function of temperature and grain size; predictions of the model are in qualitative agreement with experimental results. *Copyright © 1996 Acta Metallurgica Inc.*

1. INTRODUCTION

Twinning and slip are competing mechanisms of deformation, especially in b.c.c. metals where obstacles to available dislocation motion are often of short-range nature, resulting in a high temperature dependence of yield stress. In many metals the activation energy for twinning is very high, so that the strain rate and temperature dependence are only minor. When the stress required for twinning becomes less than the stress required for dislocation motion, plastic deformation is favoured by twinning. The study by Armstrong and Zerilli [1] shows this transition in a clear manner for iron; once the threshold stress for twinning is reached, this mechanism becomes operative. This condition also dominates at very high rates of straining, and many metals and alloys (both b.c.c. and f.c.c.) have been shown to twin profusely when deformed at high strain rates and shock loaded at pressures which exceed a critical twinning stress [2–8]. A rationale for the slip-twinning transition at high strain rates has been proposed by Meyers and Murr [8]. In f.c.c. metals and alloys, the critical twinning pressure (above which deformation twins occur for plane-wave shock loading) is stacking-fault energy dependent, increasing for increasing stacking-fault energy [9].

Tantalum, tungsten and tantalum–tungsten alloys have been of interest over the past decade because of their applications in penetrating weapons and related ballistic applications. The simplest performance parameter, the depth of penetration, is related to $(\rho_p/\rho_T)^{1/2}$ where ρ_p and ρ_T are the penetrator and target densities respectively; therefore, the high density of these metals is highly desirable. In such applications, shock deformation may play a significant role in the explosive self-forming and in the subsequent penetration process.

Previous reports of twinning in tantalum have included tensile testing in liquid nitrogen ($\sim$78 K) [10], impact testing (using a hammer!) between room temperature and liquid nitrogen temperature [11, 12], cold rolling [13], and shock loading by a glancing incidence plane wave having an estimated peak pressure of 24 GPa [14]. In this latter study of shock-loaded tantalum [14], transmission electron microscope (TEM) images showed tiny linear streaks which were contrasted with etched, linear bands in scanning electron microscope (SEM) surface views of the shocked samples, having an average grain size of 55 μm. However, no crystallographic or systematic diffraction evidence for twinning was presented. In a recent TEM study of shock-loaded tantalum and a Ta–10 w/o W alloy (having average grain sizes of 68 and 73 μm respectively), a limited amount of deformation twinning was observed in tantalum shock loaded to a peak pressure of 20 GPa (1 μs pulse duration) by Gray and Vecchio [15]; TEM evidence, including a corresponding SAD pattern containing twin reflections, was provided for a Ta–10 w/o W alloy sample. They [15] observed that the reload yield

†To whom all correspondence should be addressed.

behaviour of shock-pre-strained Ta and Ta–10 w/o W did not exhibit enhanced shock hardening when compared with their respective quasi-static stress–strain response at an equivalent strain level. Since deformation twins were observed in the shock loaded samples, but were absent in the uniaxially compressed samples deformed to an equivalent strain, twinning was not sufficient to contribute to shock hardening.

Unlike f.c.c. metals and alloys, the shock response of b.c.c. refractory metals has received only limited attention [2–4]. Wongwiwat and Murr [4] examined plane-wave shock loaded molybdenum over a range of grain sizes (1 to 67 μm) and peak pressures (14 to 35 GPa). Only at the highest pressure (35 GPa) and in the larger range of grain sizes did they observe appreciable deformation twinning, ranging from about 3 to 6 volume percent. The twins also often had a much different (lenticular) appearance from those twin-fault bundles observed in shock-loaded f.c.c. metals and alloys. In addition, the twin volume fraction increased with shock pulse duration (between 2 and 8 μs).

The objectives of this paper are (a) to report results of deformation twinning in tantalum following plane-wave shock loading to a peak pressure of 45 GPa; (b) to determine the effect of shock-induced deformation twinning on the post-shock mechanical response; and (c) to provide a rationale for the formation of twinning by shock loading.

2. EXPERIMENTAL TECHNIQUES

The tantalum used in this investigation was prepared and processed by the Cabot Corporation as 155 mm discs 8 mm thick through press forging of ingots into slabs, and subsequent cross-rolling and final annealing to produce an equiaxed [100] textured grain structure having an average grain size, as measured by the linear intercept method, of ~ 43 μm. The intestitial impurities in this material were determined by chemical analyses and are equal to, in parts per million: oxygen: 70; nitrogen: 10; carbon: 60; hydrogen: 4. They are known to have a considerable effect on mechanical response; a recent evaluation by Strutt *et al.* [16] assesses their effect. A disc specimen was shock loaded and soft-recovered using a circular Ta–2.5 w/o W flyer plate accelerated to an impact velocity of 1.29 mm μs^{-1} using a set-up developed at New Mexico Tech [17] with a plane-wave lens and a PBX 9501 main explosive charge. This arrangement produced a peak shock pressure of ~ 45 GPa at a pulse duration of ~ 1.8 μs. The impact velocity was established by four sets of velocity pins. The schematic shock-loading set-up is shown in Fig. 1. The sample, having a diameter of 76 mm and thickness of 7.2 mm, was inserted in the centre of a tantalum–tungsten alloy plate. Eight samples with 32 mm diameter surrounded the central specimen (used in the present investigation). The central plate had recesses bored so that the nine disc-shaped specimens were placed into them. A protective cover plate (1.6 mm thick tantalum) was riveted (using Ta) to the disc containing the specimens. A tantalum momentum trap, placed on top of two steel momentum traps, was used to capture the reflected tensile pulses. Lateral tantalum and steel rings were used to capture the lateral release waves. Great care was taken to ensure a state of uniaxial strain in the specimen and reflected tensile pulses were trapped. This is important, since it has been shown by Mogilevsky and Teplyakova [18] and Gray *et al.* [19, 20] that residual strains have a significant effect on the microstructure and strengthening of copper. The gaps between tantalum discs (specimens) and tantalum plates were kept at a minimum. The tantalum–tungsten plate that encased the specimens had a higher flow stress than the tantalum (central) specimen and therefore the lateral flow of the specimen during shock compression is inhibited. The pressure was calculated from the known equation of state for tantalum (relation between shock and particle velocities) [21] and the impedance-matching method, using the experimentally measured impact velocity. Specimens were trepanned from the shock loaded disc by electro-discharge machining for quasi-static uniaxial compression testing. Similar samples were extracted from an unshocked disc of the same material for comparison. Compression testing was performed between about 0.22 and 0.40, consistent with the transient strain undergone by shock loading. Quasi-static strain rates of 2.5×10^{-4} to 2.5×10^{-3} s^{-1}, were achieved using a screw-driven Instron testing machine and a dynamic strain rate of nominally 3×10^{3} s^{-1} was achieved using a split-Hopkinson pressure bar.

A digital Vickers microhardness tester was used to measure the residual hardness values for the experimental samples using a 200 gf load. Standard metallographic sections of all experimental samples were prepared for light microscopy where the grain structure was revealed by etching in a solution composed of 4 parts HCl, 2 parts HNO_3 and 8 parts HF at ice temperature (~ 0°C). Standard 3 mm disc samples were prepared for electro-thinning for transmission electron microscopy using a Struers Tenupol III jet electropolisher. An electropolishing solution consisted of 90 ml HF, 270 ml H_2SO_4, 300 ml glycerol, and 1500 ml methanol at 10°C; using 8–10 V as the electropolishing condition. A Hitachi H-8000 analytical transmission electron miscroscope equipped with a double-tilt stage was employed utilizing 200 kV accelerating voltage in the CTEM mode.

3. RESULTS AND DISCUSSION

3.1. *Characterization of the shocked material*

Although there was some variability in the propensity of twinning through the sample disc, it

was often observed that deformation twinning was somewhat more profuse near the impact surface in the shock loaded sample, and in some regions there was almost no twinning near the rear sample surface. This feature is illustrated in the light microscope views of etched front and rear surface samples along a cylindrical specimen extracted from the shock loaded sample shown in Fig. 2. Figure 2(a), corresponding to the impact surface shows that essentially every grain contained deformation twins, if in fact the etched markings are uniformly representative of deformation twins. This orientation and the preponderance of (100) grain surfaces is consistent with pre-shock texture mappings [22]. These features are more clearly and convincingly demonstrated in the enlarged light microscope view of two adjoining (100) grains shown superimposed upon a bright-field image typical of the deformation twins observed in the TEM (Fig. 3). The SAD pattern insert illustrates the (100) grain surface orientation in the TEM image and establishes the ⟨024⟩ twin trace directions for the four different, principal {112} twin

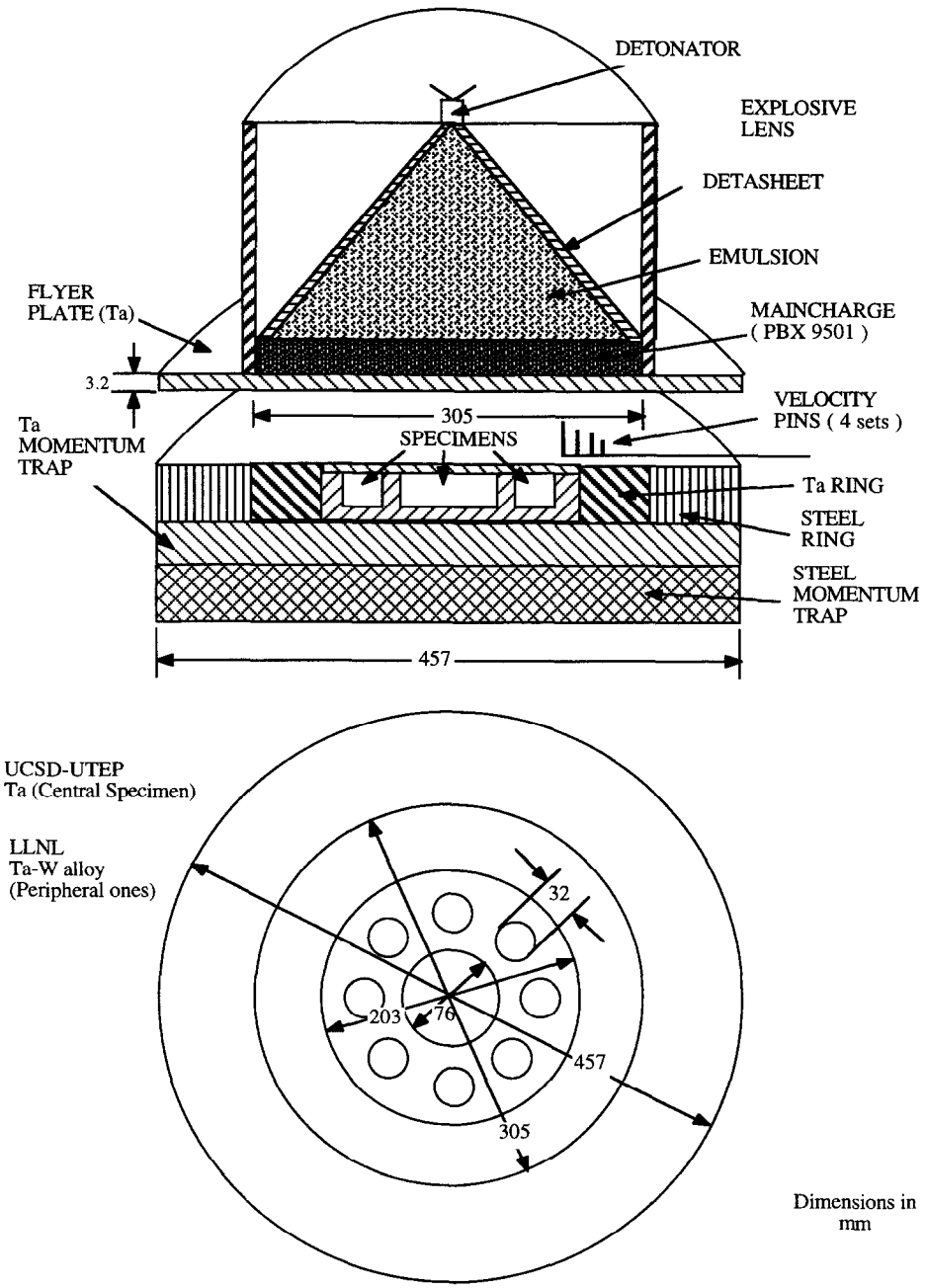

Fig. 1. Experimental set-up used to generate shock-wave propagation with amplitude of 45 GPa through Ta and Ta–W specimens.

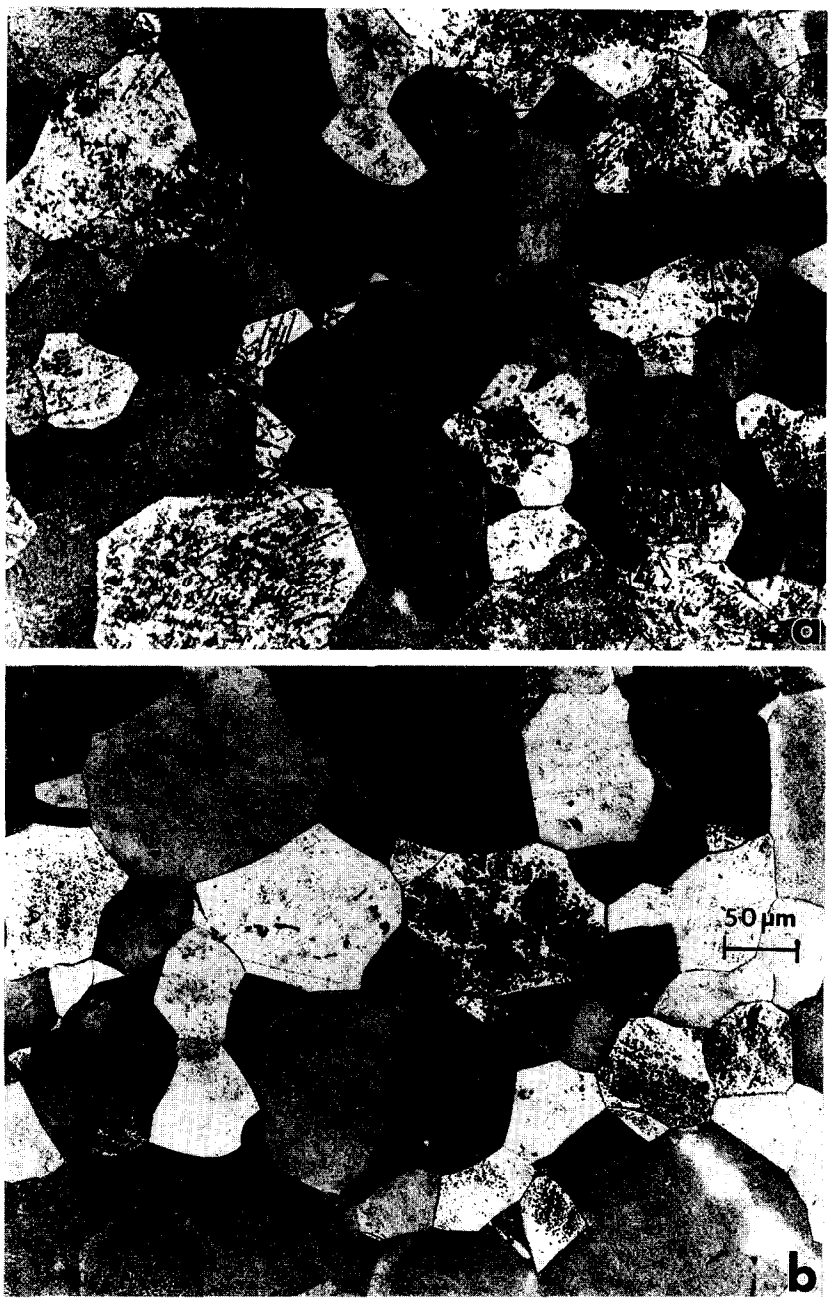

Fig. 2. Optical metallograph views of the front (impact) (a) and rear (b) sample surfaces for plane-wave shock loaded tantalum.

planes shown. It can also be noted that the longer etched segments and short etched regions in the light microscope views in both Figs 2 and 3 are represented by very short and considerably larger twin segments. The fact that there are no prominent twin reflections in the corresponding SAD pattern in Fig. 3, in spite of the fact that the twins along each $\langle 042 \rangle$ twin trace direction are rather strongly diffracting, is a consequence of the fact that the twin planes make the same angle with the surface and occur in two sets whose traces are perpendicular in the (100) surface plane; therefore, the ideal twin reflections coincide with those of the (100) matrix. However, because of the irregular (lenticular) twin shape, and their irregular volumes and often overlapping twin planes, additional, kinematic reflections can occur in the diffraction pattern depending upon specific, operating twin shape transforms [23]. In addition, the preponderance of the twins along each of the four different directions in the TEM image of Fig. 3 exhibit a very similar projection width, indicative of the uniformity of many microtwins along a single $\{112\}$ plane segment, and also attesting to the fact that all of the $\{112\}$ planes make an angle of $\sim 66^\circ$ with the (100) surface plane. Notable exceptions occur at (1) and (2) in the TEM image. At (1), the

twin plane is somewhat irregular while at (2), there are two different {112} planes, $(11\bar{2})$ and $(\bar{1}1\bar{2})$, inclined opposite to one another, but each making an angle of $\sim 66^\circ$ with the (100) specimen surface, and presenting the chevron-appearing segment observed. This {112} twin orientation confirms earlier experimental determinations by Barrett and Bakish [11], Anderson and Bronisz [12], Jagannadham *et al.* [24]

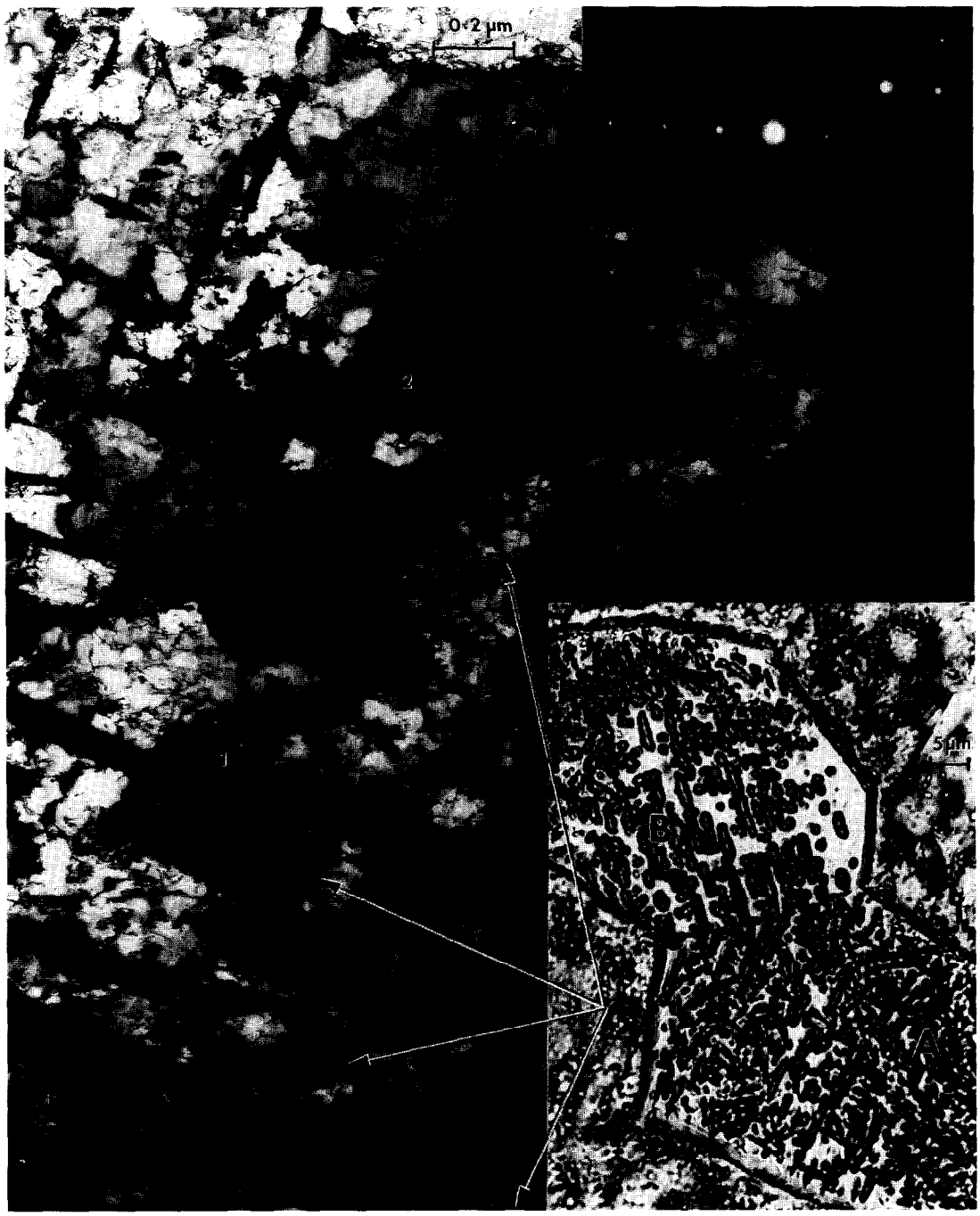

Fig. 3. Composite views of deformation twins in shock loaded tantalum. An enlarged light microscope view of adjoining, etched, (100) grains near the impact surface of shock-loaded Ta is superimposed upon a bright-field TEM image of twins in a corresponding (100) orientation indicated in the SAD pattern inserted top right. The superimposed optical metallographic view is oriented so that the etching trace directions in grain A coincide with the four twin race directions noted in the TEM image. The SAD pattern shows a two-beam diffraction condition for the matrix with $\vec{g} = [031]$.

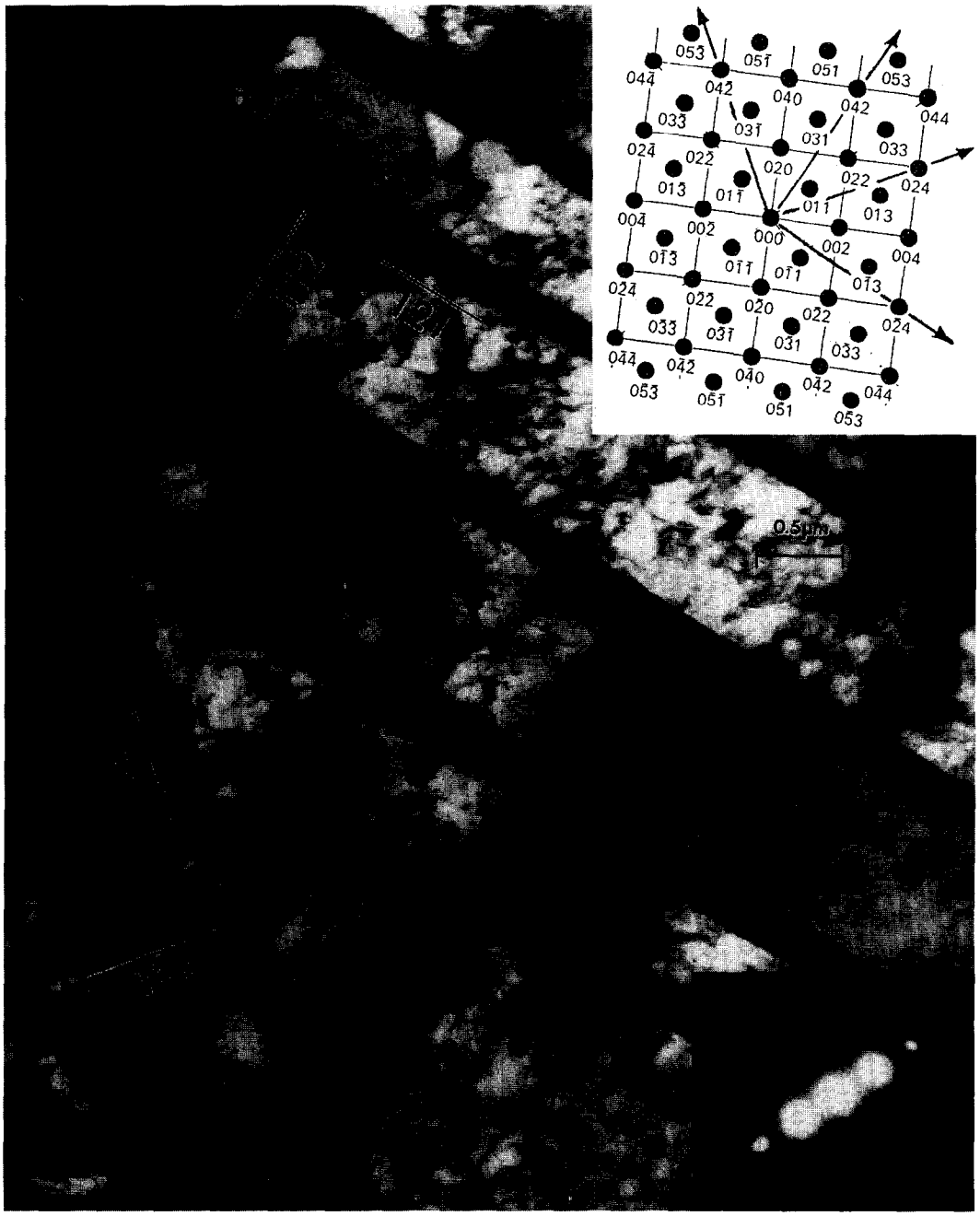

Fig. 4. TEM bright-field image of linear {112} microtwins in (100) shock-loaded tantalum showing superimposed, indexed diffraction net (top right) and corresponding SAD pattern (lower right). Specific {112} traces along ⟨024⟩ directions (shown in the diffraction net) are indicated. The SAD pattern shows a three-beam diffraction condition for the matrix with $\pm\bar{g} = [011]$.

(for Ta–10 at.% Nb), and Gray and Vecchio [15]. Of these, only Gray and Vecchio [15] used shock waves to induce mechanical twinning.

The crystallographic and geometrical features of deformation twinning in Ta described for Fig. 3 are perhaps more clearly delineated in Fig. 4 which shows a preponderance of longer twins along the $[0\bar{2}4]$ direction for a (100) grain, where the twin projections consist of two overlapping (112) planes or (112) microtwins, and twins occur along all four of the ⟨024⟩ trace directions noted in the indexed (matrix) diffraction net for the (100) grain surface orientation (corresponding to a [100] b.c.c. zone axis). The SAD pattern insert for the corresponding bright-field TEM image area shown in Fig. 4 is, like that shown for Fig. 3, devoid of kinematical twin reflections, and, as a consequence, the prominent twin reflections coincide with those of the (100) matrix. Specific twin

reflections corresponding to (112), for example, occur in every third layer with reference to [011] in the Fig. 4 insert. That is, $[0\bar{1}\bar{1}]$ through [011] and $[02\bar{4}]$ through $[04\bar{2}]$, etc. The twin zone axis for twinning on (112) is $[\bar{2}12]$. Correspondingly, similar conditions apply to the other three principal {112} twinning planes with $\langle 04\bar{2}\rangle$ traces in the [100] matrix zone. Two sets of twins produce coincident twin reflections along $[01\bar{1}]$ and each third, parallel row, while two sets of twins produce the same coincident array of twin spots along [011], at 90°.

These features of b.c.c. twin reflections ($\langle hkl\rangle/3$) reciprocal lattice reflection conditions) were described earlier by Wayman and Bullough [25, 26], and the occurrence of kinematical (extra) rel-rod reflections arising from the foil geometry and twin shape transforms, are more clearly and unambiguously illustrated in Fig. 5, which shows twins in a (311)

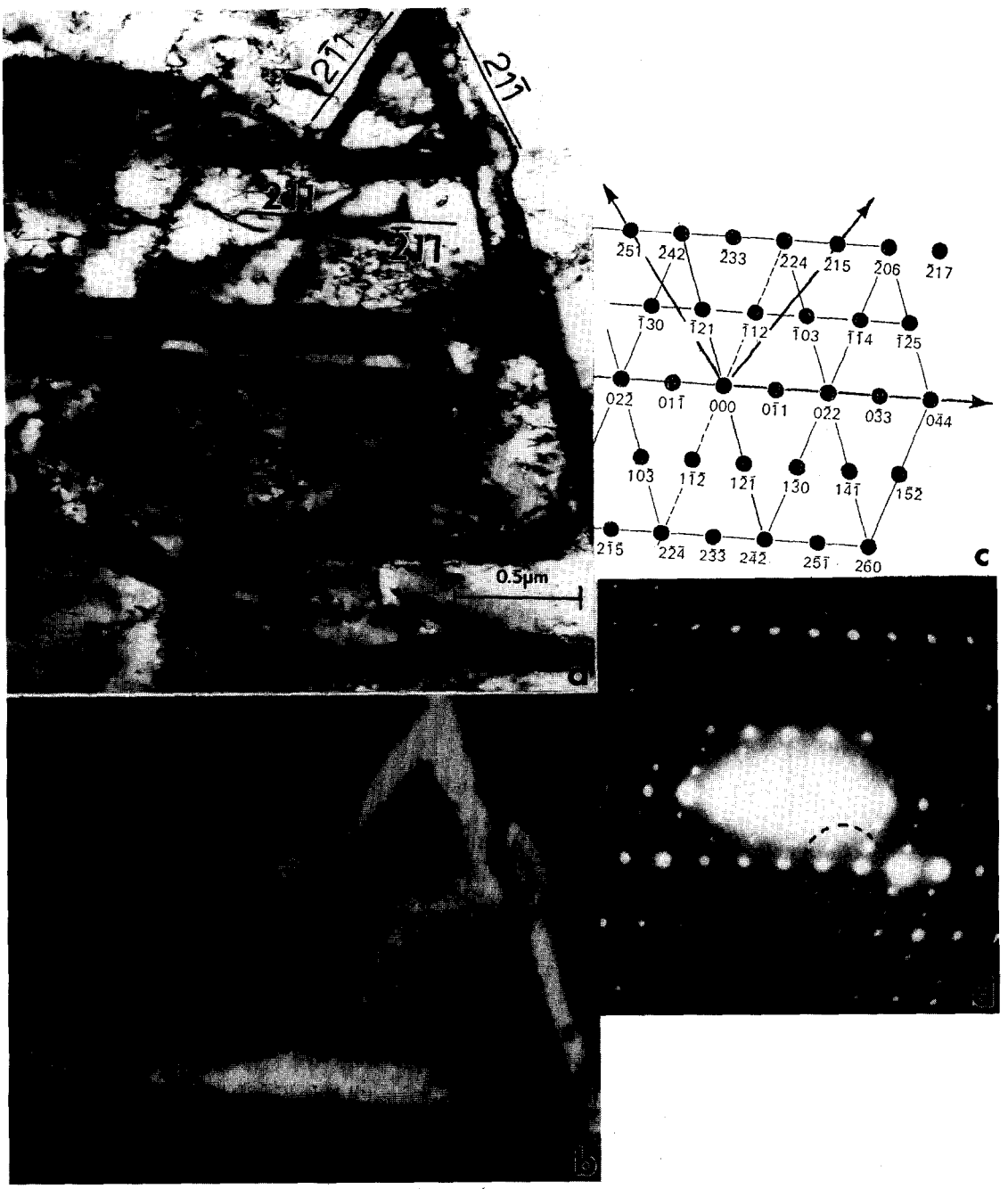

Fig. 5. Bright-field (a) and dark-field (b) TEM images for deformation microtwins in (311) shock-loaded tantalum. The corresponding twin reflections utilized in the aperture dark-field image in (b) are circled in the SAD pattern insert in (d). The corresponding {112} twin planes are noted in (a) for trace directions shown in the indexed diffraction net inserted upper right (c).

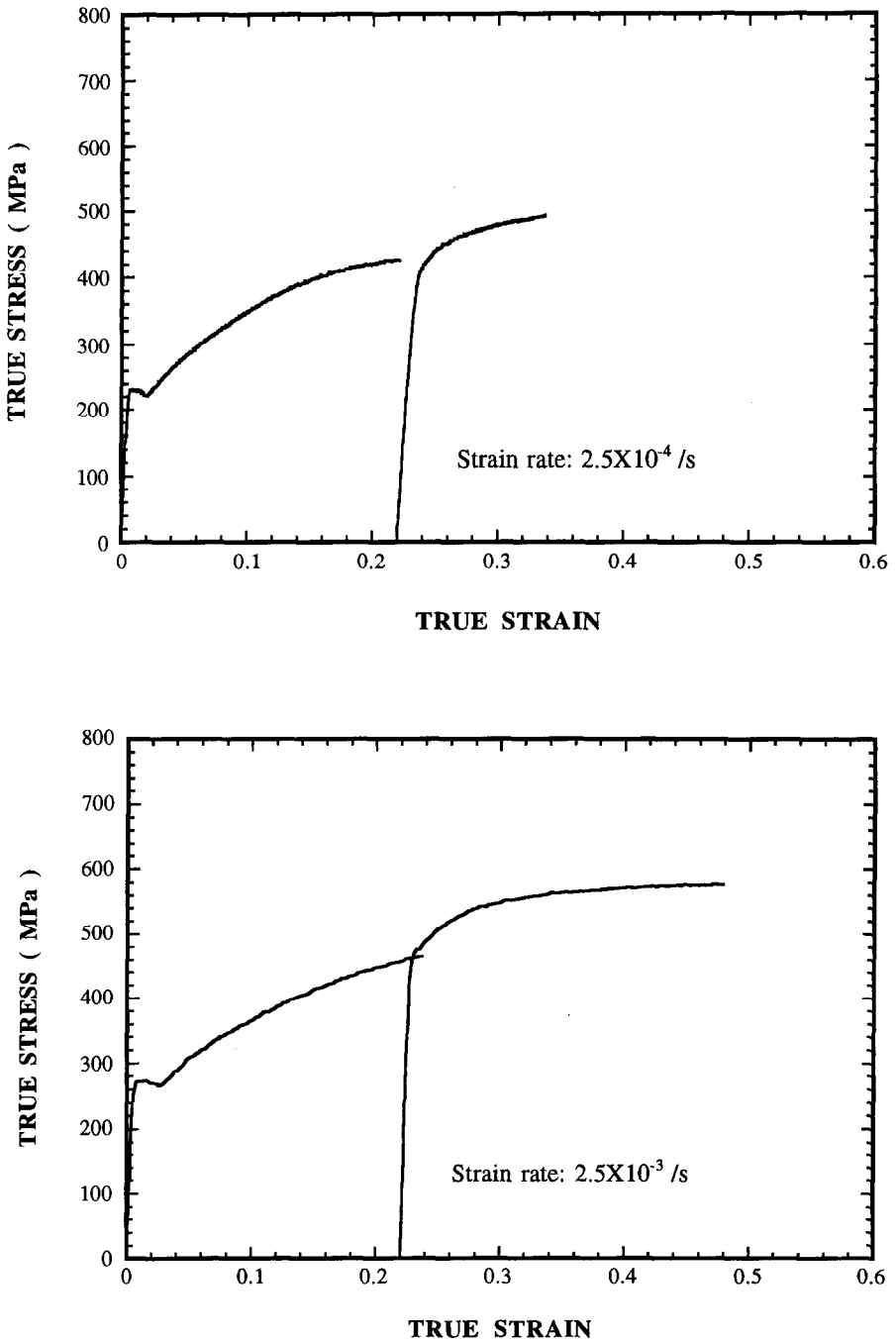

Fig. 6. Quasi-static stress–strain response of as-received and shock-pre-strained (45 GPa) tantalum. The reload curves are offset on the stress–strain axis by the transient strain due to the shock pre-strain ((4/3)ln(V/V_0)@ − 22%). (a) Strain rate of $\sim 10^{-4}\,s^{-1}$. (b) Strain rate of $\sim 10^{-3}\,s^{-1}$.

orientation, with prominent twin and double diffraction spots occurring as continuous, reflection layers corresponding generally to $\langle 112\rangle/3$. (That is, if a twin spot occurs at $\langle 112\rangle/3$, then the double diffraction spot occurs corresponding at $\langle 112\rangle$ 2/3, etc.) Here, kinematical twin and double diffraction reflections corresponding to twinning on $(21\bar{1})$ and $(2\bar{1}1)$ planes, which each make an angle of $\sim 42°$ with the (311) grain surface, occur at $\langle 112\rangle/3$ positions while twin spots corresponding to (211) and $(\bar{2}11)$ planes along the $[0\bar{1}1]$ direction coincide with the corresponding matrix reflections in each third reflection layer. Prominent twin and double diffraction spots occur in rows parallel to $[\bar{1}12]$. The reflections along $[\bar{1}12]$ are, in fact, all double diffraction spots which alternate every third row.

Between these rows, the twin and double diffraction spots alternate [26]. Figure 5 provides unambiguous proof for deformation twinning in shock deformed Ta since the dark-field image includes all prominent twin reflections along each of the three twin trace directions for the (311) orientation. The bright-field and corresponding dark-field images in Fig. 5 also clearly illustrate the twin-plane geometries corresponding to $\sim 42^\circ$ inclinations relative to (311) along $[\bar{2}51]$ and $[\bar{2}15]$, and a correspondingly wide projection for (211) along $[0\bar{1}1]$ which makes an angle of only $\sim 10^\circ$ with the (311) surface plane.

3.2. *Post-shock mechanical response*

The post-shock mechanical response was assessed by means of quasi-static and dynamic compression tests and microhardness measurements. The stress–strain responses of as-received and shock loaded tantalum were compared by assessing the total transient effective strain imparted by shock loading through the expression (e.g. [27]):

$$\epsilon_s = \frac{4}{3} \ln \frac{V}{V_0}, \tag{1}$$

where V and V_0 are the shock and initial specific volumes. The pressure of 45 GPa generates a corresponding specific volume, V, equal to 50.08 $cm^3\,kg^{-1}$; V_0 is equal to 60.04 $cm^3\,kg^{-1}$. These values are obtained by the application of the Rankine–Hugoniot relations to the equation of state for tantalum [21]. The corresponding effective shock strain ϵ_s, is 0.22. Equation (1) incorporates the strains at both the shock front and release portion of the wave. The same effective strains were assumed in shock and uniaxial compression. The results of mechanical tests at 2.5×10^{-4} and $2.5 \times 10^{-3}\,s^{-1}$ are shown in Fig. 6. The curves for the shocked material are displaced in the plastic strain axis by the amount of 0.22. The hardening imparted by shock exceeds the one produced by normal work hardening. Similar results were obtained at high strain rates; the analysis is complicated by the fact that the stress–strain curves are adiabatic under these conditions and reflect the thermal softening produced by the temperature rise. Thus, interrupted (incremental) tests were carried out for both the as-received and shocked materials and the curves obtained by these tests are shown in Figs 7(a) and (b), respectively. The specimen was allowed to cool to room temperature after each load increment. This procedure was initially introduced by Wittman *et al.* [28] and was further developed by Nemat-Nasser and Isaacs [29]. The quasi-isothermal curves which form the envelope of the interrupted tests are obtained by using a modified form of the Johnson–Cook equation with parameters established as described by Meyers *et al.* [22]. For the shocked condition, the same softening and strain-rate sensitivity parameters were retained. The following equation was used,

$$\sigma = (\sigma_0 + B\epsilon^n)\left[1 + C\left(\log_{10} \frac{\dot{\epsilon}}{\dot{\epsilon}_0}\right)\right] e^{-\lambda(T - T_r)}. \tag{2}$$

The values of the parameters σ_0, B, n, C, $\dot{\epsilon}_0$, T_r and λ are given in Table 1. T_r and $\dot{\epsilon}_0$ are reference temperature and strain rate, respectively.

Figure 8 shows the comparison of the quasi-isothermal curves for unshocked and shocked conditions. The flow stress of the shocked material exceeds the one of the work-hardened (to $\epsilon = 0.22$) as-received material significantly (by $\sim 50 - 100$ MPa); importantly, the work-hardening coefficient of the shocked material is much higher than the as-received. These differences are attributed to the mechanical twinning which partially sub-divides the grains and thereby increases the flow stress of the material.

The differences obtained in the mechanical tests are confirmed in microhardness measurements. The average in-plane Vickers microhardness for the as-received tantalum sample was 1.06 GPa while that for the shocked sample was 1.76 GPa. The front and rear surface hardness for the shocked sample did not vary by more than ± 0.02 GPa. The average Vickers microhardness for the uniaxially compressed, as-received sample deformed quasi-statically by 23% was measured in the plane perpendicular to the compression (strain) axis to be 1.56 GPa. Correspondingly, the Vickers microhardness of a shocked sample and subsequently uniaxially compressed by 26%, was 1.9 GPa. These microhardness comparisons indicate there is significant (enhanced) shock hardening at a peak shock pressure of 45 GPa in comparison with quasi-static uniaxial stress compression to the same effective strain. The residual, incremental hardness change between the as-received Ta and the shock loaded Ta was about 0.7 GPa, whereas, it was about 0.54 GPa between the as-received and uniaxially compressed samples (for both the quasi-static and dynamic reload cases).

An examination of the residual microstructures following uniaxial compression of the unshocked, starting material failed to reveal any deformation twins, but the dislocation density was substantially increased. The quasi-statically loaded Ta exhibited fairly well formed dislocation cell structures. These cell structures were even more dense in the dynamically deformed, unshocked sample where the strain was considerably larger (-40%); in addition, linear features coincident with {100} slip plane traces occurred. Indeed, the dislocation density was increased only slightly in the pre-shock loaded and quasi-statically compressed tantalum as well, and these features are illustrated generally in the comparative views shown in Fig. 9. In order to render the comparisons as meaningful as possible in Fig. 9,

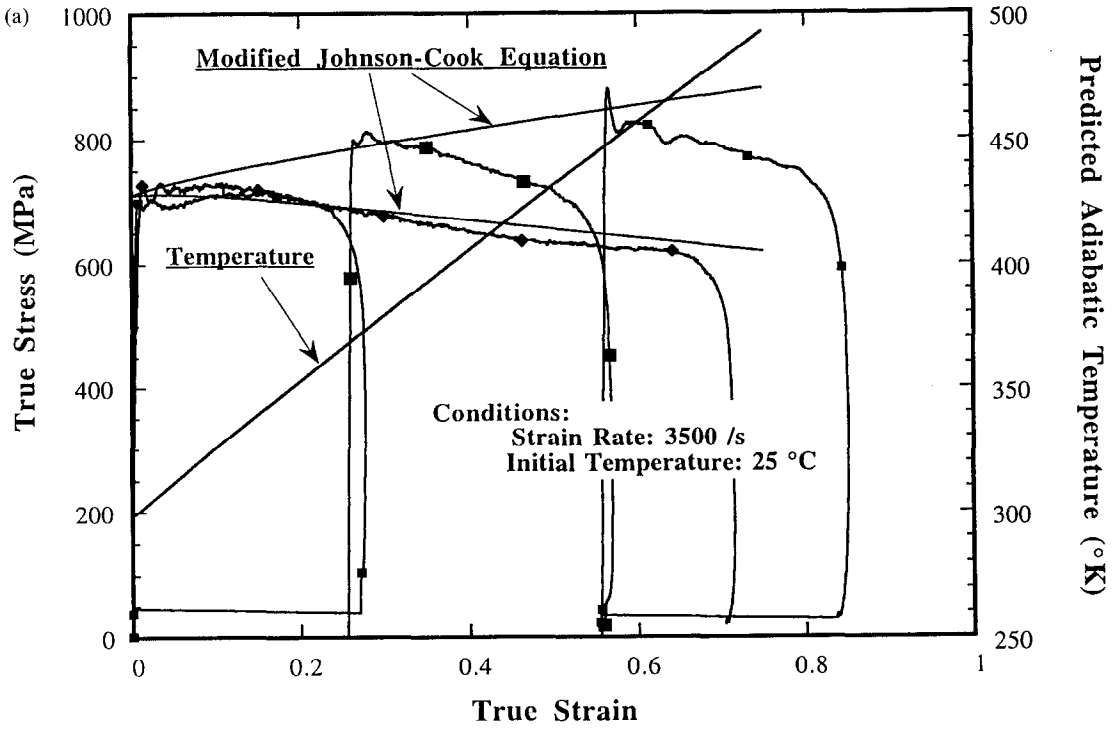

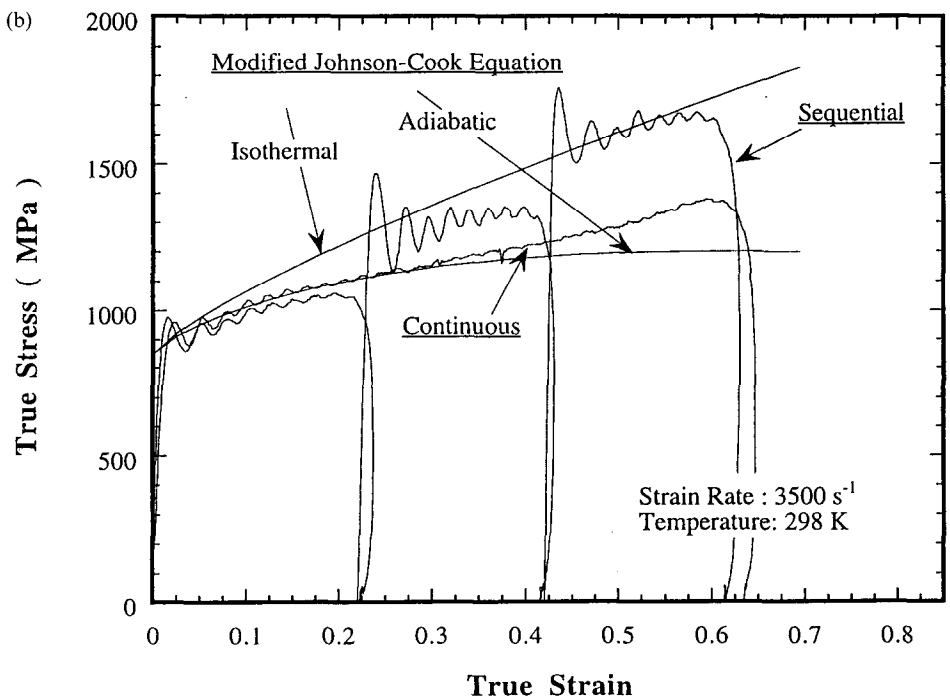

Fig. 7. High-strain-rate ($3.5 \times 10^3\ s^{-1}$) stress–strain responses of (a) as-received and (b) shocked (45 GPa) tantalum. Isothermal curves constructed from adiabatic curves by use of equation (2); they form an envelope for incremental curves.

Table 1. Constitutive equation parameters

Parameter	As-Received	Shocked
σ_0	684.5 MPa	850 MPa
B	205.3 MPa	1300 MPa
n	0.78	0.78
C	0.1	0.1
$\dot{\epsilon}_0$	3500 s^{-1}	3500 s^{-1}
T_r	298 K	298 K
λ	0.0014	0.0014

the magnification of all TEM images is the same and all but two of the surface orientations were (100): $\hat{\mathbf{g}} = [020]$.

While the specific feature of shock hardening is not obvious, either for the current observations in shocked Ta or other similar observations, especially in f.c.c. materials, there is obviously a rapid rise in dislocation density and interactions, a kind of strain-rate induced saturation of dislocation density. Indeed, the fact that in the current experiments the peak shock pressure was so much higher than any previously reported examples of shock loading of Ta is an indication of the fact that very high pressure, high-strain-rate loading may significantly alter the fundamental dislocation processes. Large strain, even at quasi-static strain rates, may also significantly alter dislocation processes. Some evidence for this phenomenon may be manifested in the significantly different TEM observations for unalloyed Ta in the work of Gray and Vecchio [15] in contrast to the comparisons of dislocation and twin microstructures in Fig. 9 of the present work. No long, straight, screw dislocation segments were observed for quasi-static loading where the strains were in excess of −20%. Consequently, there did not appear to be significant restrictions on cross slip. Figure 10 provides an example of this phenomenon for the dynamically loaded (at −40%) unshocked Ta where the microstructure is composed primarily of dislocation cells with well-defined slip features superimposed on this microstructure along traces of {110} planes. These slip-related features (especially visible in Fig. 10(a)) are not deformation twins; they do not coincide with the twinning features noted, for example, in Figs 3 or 4. It is clear that there is a dramatic shift in the slip/shear plane when twinning occurs. Consequently, while there may be some cross-slip suppression in Ta at lower peak shock pressures and lower strains, there are apparently some fundamental differences in the stored dislocation density in Ta at low strains or low shock pressures (<25 GPa). The fact that the reload yield behaviour of unalloyed Ta shock prestrained to 7 GPa at 218 or 410°C in the previous work of Gray and Vecchio [15] exhibited increased hardening compared with shock pre-straining at ambient temperature in effect supports this contention; different rate controlling mechanisms can be activated.

3.3. *Constitutive model for the slip-twinning transition*

A rationale for the slip-twinning transition at high strain rates is presented below. It is an extension of

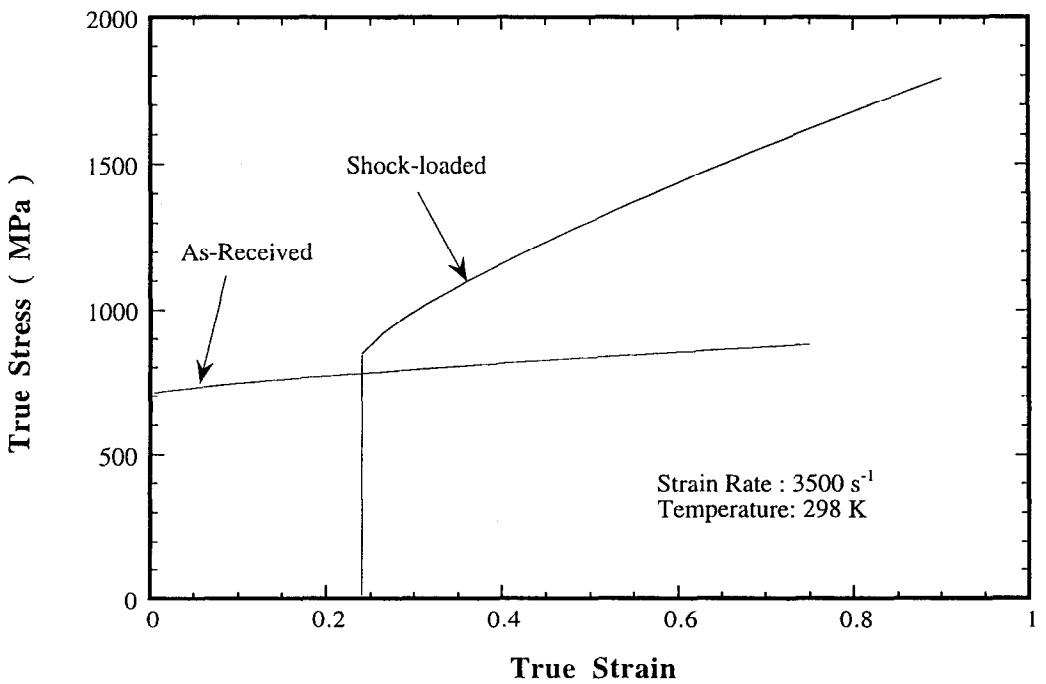

Fig. 8. Comparison of isothermal stress–strain responses of as-received and shocked tantalum at $3.5 \times 10^3\ s^{-1}$.

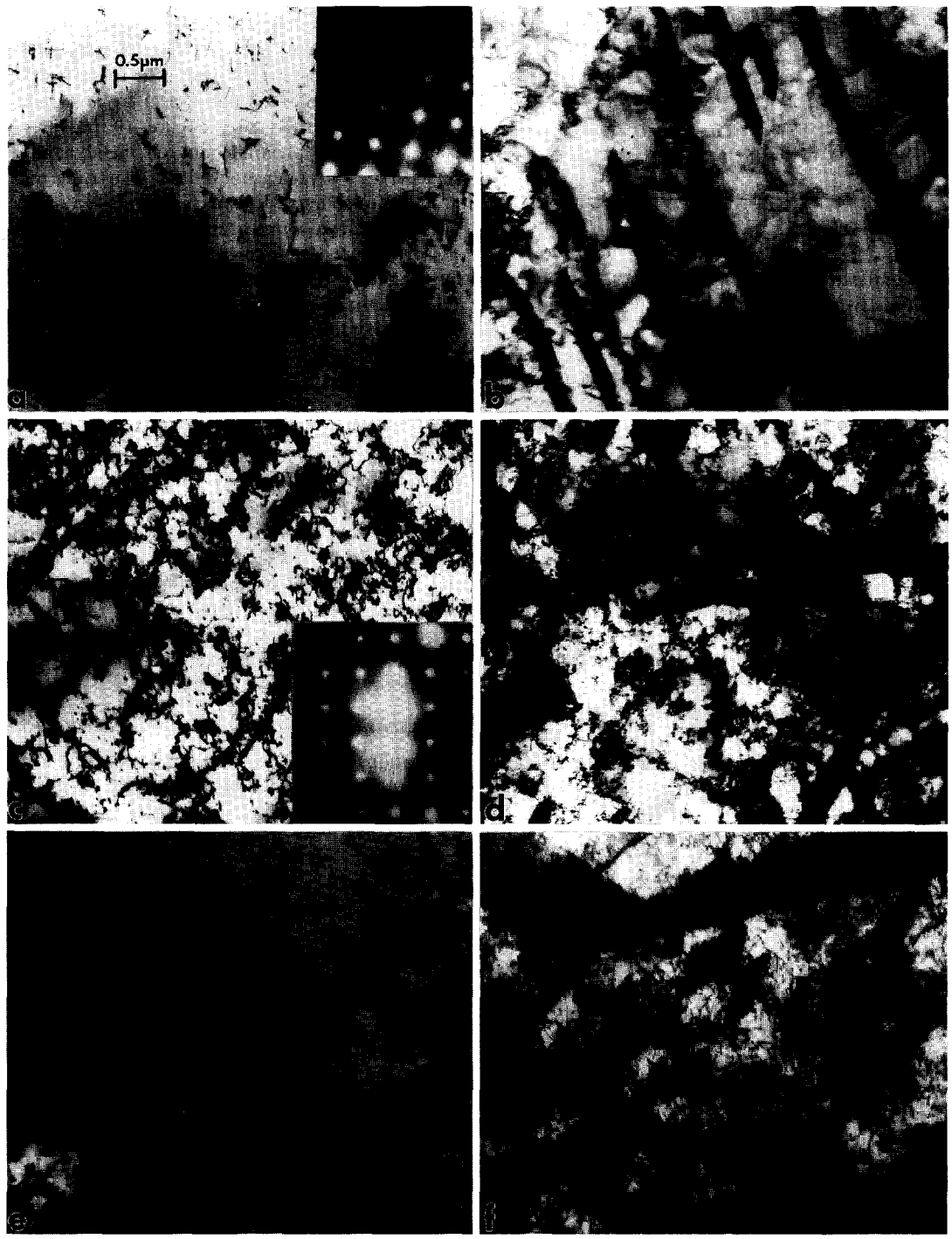

Fig. 9. TEM micrographs comparing dislocation substructures in all experimental tantalum samples. (a) As-received material (undeformed). (b) Shocked (45 GPa) material. (c) As-received quasi-statically deformed (-23%; $\sim 10^{-4}\,s^{-1}$). (d) Pre-shocked and quasi-statically deformed (-26%; $\sim 10^{-4}\,s^{-1}$). (e) As-received, dynamically deformed (-39%; $\sim 10^{3}\,s^{-1}$). (f) Pre-shocked, dynamically deformed (-27%; $\sim 10^{3}\,s^{-1}$). All grain surface orientations are (100) except (e) and (f) which are (111). Operating reflections are $\vec{g} = [020]$ except (e) and (f) where $\vec{g} = [0\bar{1}1]$. Magnifications are the same and are shown in (a).

initial considerations developed by Meyers *et al.* [30], who observed that the incidence of twinning in shock-loaded copper was dependent on grain size. Armstrong and Worthington [31] were the first to develop a constitutive relation for metals undergoing plastic deformation by twinning. This constitutive relation incorporated strain, strain rate, temperature, and grain size, and addressed experimental observations. The recent study by Song and Grady [32] shows how the twin-slip transition occurs in

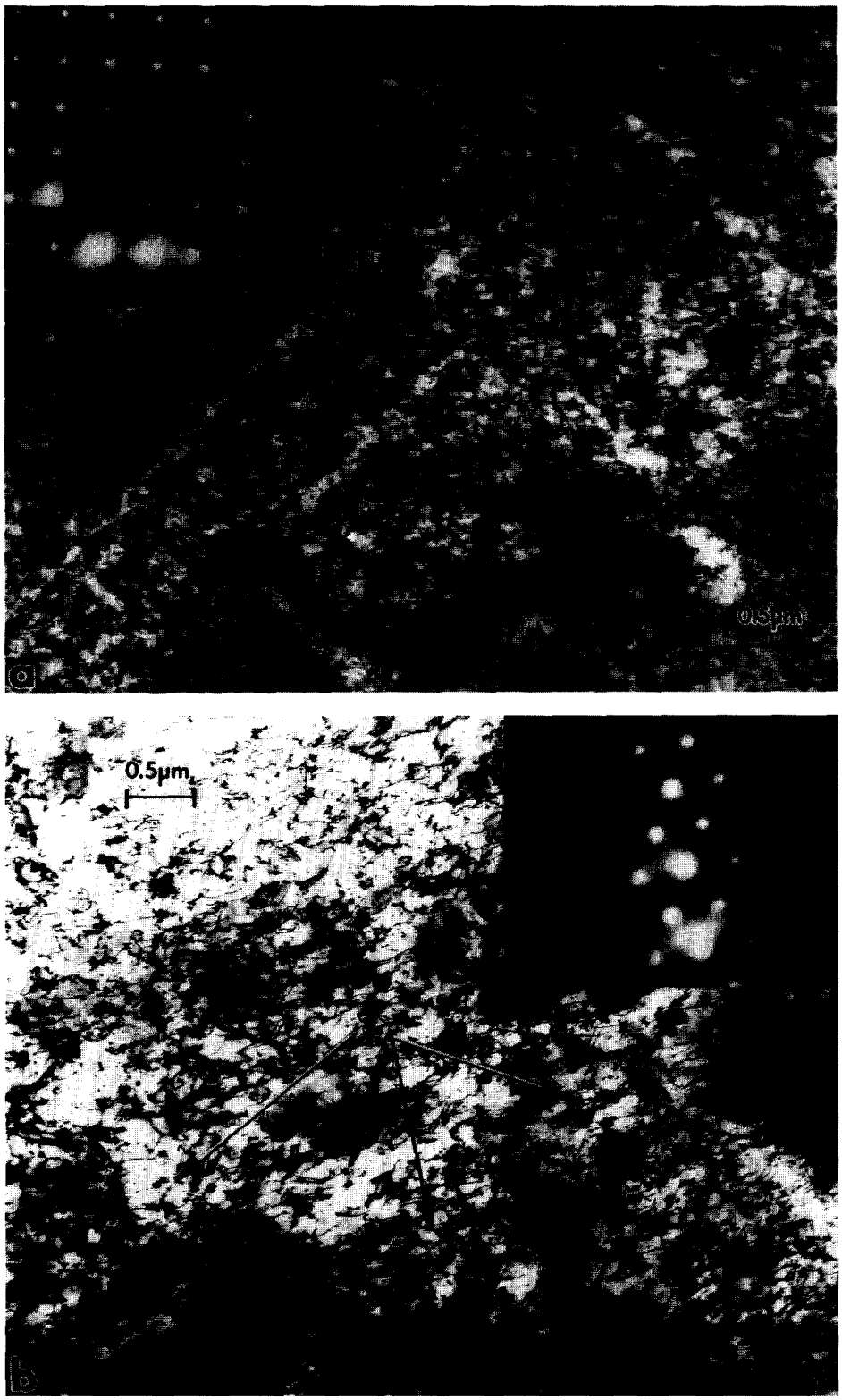

Fig. 10. TEM, bright-field images showing linear slip/shear features coincident with {101} slip plane traces in ⟨020⟩ directions in a (100) oriented grain. (a) As-received, unshocked Ta dynamically deformed −40% in Hopkinson bar. The specimen was prepared from a section perpendicular to the strain/impact axis. (b) A different (111) orientation for the same conditions. Linear features are shown along ⟨112⟩ directions coincident with $\{11\bar{0}\}$ slip planes.

Table 2. Schmid factors (m) for ({112}⟨111⟩) twinning; [100] and [111] textures[a]

Twin plane	Twin direction	M for [100]	M for [111]
112	$\bar{1}\bar{1}1$	−0.236	−0.314
112	$11\bar{1}$	0.236	0.314
$11\bar{2}$	111	0.236	0.000
$11\bar{2}$	$\bar{1}\bar{1}\bar{1}$	−0.236	0.000
$1\bar{1}2$	$1\bar{1}\bar{1}$	0.236	−0.157
$1\bar{1}2$	$\bar{1}11$	−0.236	0.157
$\bar{1}12$	$\bar{1}1\bar{1}$	0.236	−0.157
$\bar{1}12$	$1\bar{1}1$	−0.236	0.157
211	$\bar{1}11$	−0.471	0.314
211	$1\bar{1}\bar{1}$	0.471	−0.314
$\bar{2}11$	111	−0.471	0.000
$\bar{2}11$	$\bar{1}\bar{1}\bar{1}$	0.471	0.000
$2\bar{1}1$	$11\bar{1}$	0.471	0.157
$2\bar{1}1$	$\bar{1}\bar{1}1$	−0.471	−0.157
$21\bar{1}$	$1\bar{1}1$	0.471	0.157
$21\bar{1}$	$\bar{1}1\bar{1}$	−0.471	−0.157
121	$\bar{1}1\bar{1}$	−0.236	−0.314
121	$1\bar{1}1$	0.236	0.314
$\bar{1}21$	$11\bar{1}$	−0.236	0.157
$\bar{1}21$	$\bar{1}\bar{1}1$	0.236	−0.157
$1\bar{2}1$	111	0.236	0.000
$1\bar{2}1$	$\bar{1}\bar{1}\bar{1}$	−0.236	0.000
$12\bar{1}$	$\bar{1}11$	−0.236	0.157
$12\bar{1}$	$1\bar{1}\bar{1}$	0.236	−0.157

[a]It is assumed that the system with the highest resolved shear stress is activated; it is recognized that this is, in the case of twinning, a simplification.

zirconium at low strain rates; they demonstrate that the threshold stress for twinning has a very low (if any) temperature dependence. Armstrong and Worthington [31] recognized two very important effects:

(a) the necessity of micro-slip for twin initiation;
(b) the large grain-size dependence of the twinning stress. Indeed, it has been observed that the Hall–Petch slope for twinning is much higher than the one for slip for f.c.c. metals [32–38]; it has been found by Vöhringer [39] significantly to exceed the one for slip for copper; $k_T = 0.7\ \text{MN m}^{-3/2}$ and $k_s \cong 0.35\ \text{MN m}^{-3/2}$, where k_T and k_s are the Hall–Petch slopes for twinning and slip, respectively.

Recent evidence by Song and Gray [32] suggests that the Hall–Petch slope for twinning ($k_T \cong 2.4\ \text{MN m}^{-3/2}$) is ten times the one for slip [40] ($k_s \cong 0.25\ \text{MN m}^{-3/2}$). The different Hall–Petch slopes have their origin in different mechanisms responsible for the grain size effects in slip and twinning. In twinning, the stress concentration produced by a pile-up concept was used by Armstrong and Worthington [31] as the foundation for the analysis. For slip, several proposals have been advanced, starting with the classic works of Hall [41] and Petch [42], Cottrell [43], and others. Interestingly, the works by Hall [41], Petch [42], and Cottrell [43] are based on pile-ups, and would therefore predict $k_s = k_T$. Hence, the more contemporary observations by Murr and Hecker [44], and the analysis by Meyers and Ashworth [45], based on alternative mechanisms (a grain-boundary region with high dislocation density and elastic anisotropy effects) would clearly predict different slopes. The principal elements of Armstrong and Worthington's [31] analysis are presented below. Figure 11 shows a pile-up at a grain-boundary and the formation of a twin in the neighbouring grain. The orientations of pile-up and twin are marked as θ_s, λ_s and θ_T, λ_T, respectively. The stress at the tip of a pile-up with n dislocations is given as (where τ is the applied shear stress):

$$\tau_0 = n\tau. \tag{3}$$

Assuming that the dislocation source is at the centre of the grain, the external loop will have a radius $d/2$, d being the grain size. The number of loops in the pile-up is given by:

$$n = \frac{C_1 \tau d}{Gb}, \tag{4}$$

C_1 is a constant, G the shear modulus, and b the Burgers vector. Assuming that the stress at the tip of the pile-up is the local stress required to trigger twinning, then the global stress for twinning, τ_T, is expressed as:

$$\tau_T = \left(\frac{Gb\tau_0}{C_1}\right)^{1/2} d^{-1/2}. \tag{5}$$

The shear stress, τ, can be converted into a normal stress, σ, by the use of an orientation factor m; a frictional stress σ_0 is also added. This orientation

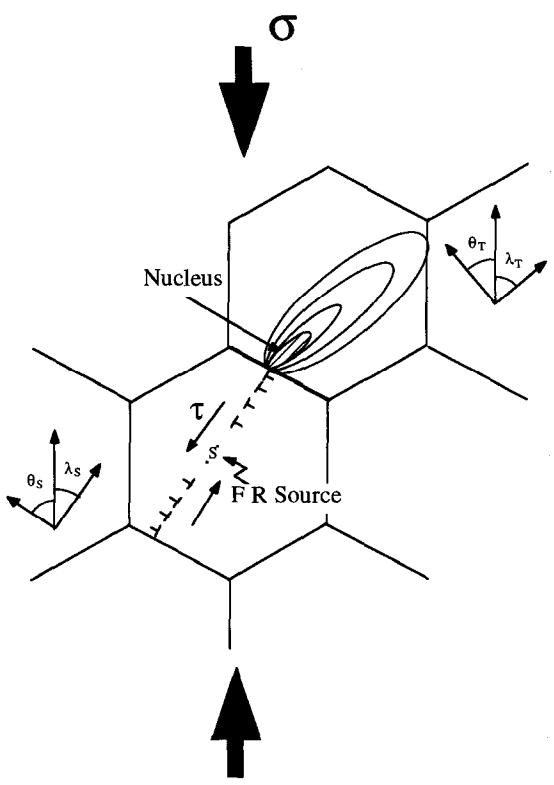

Fig. 11. Schematic representation of twin nucleation by stress concentration produced by dislocation pile-up at grain boundary.

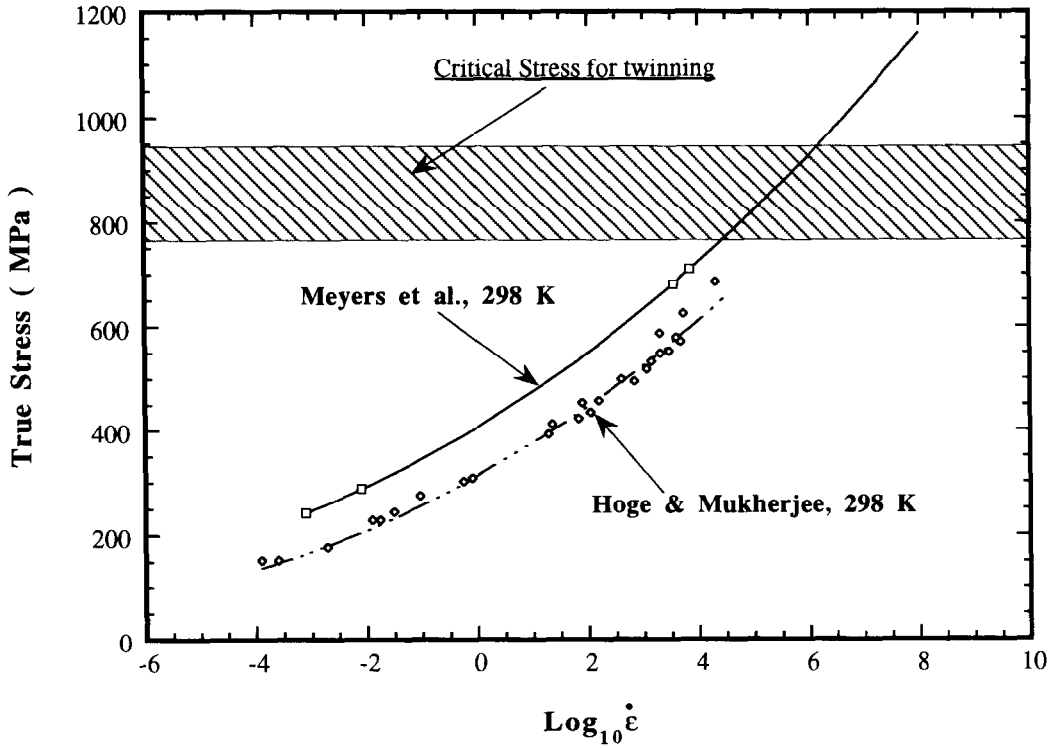

Fig. 12. Effect of strain rate on the yield stress of tantalum; results by Meyers *et al.* [18] and Hoge and Mukherjee [49]; quadratic fit used in extrapolation.

factor takes into account the angles θ_s and λ_s with the loading axis

$$\sigma_T = \sigma_0 + m\left(\frac{Gb\tau_0}{C_1}\right)^{1/2} d^{-1/2}. \quad (6)$$

The local shear stress required for twinning, τ_0, has a temperature (T) and strain-rate ($\dot{\epsilon}$) dependence that was expressed by Armstrong and Worthington [31] as:

$$\sigma_T = \sigma_0 + m\left(\frac{Gb}{C_1}\right)^{1/2}\left[\frac{U^*}{RT}\ln\frac{\dot{\epsilon}}{\dot{\epsilon}_0}\right]^{1/q} d^{-1/2}$$

$$= \sigma_0 + k_T d^{-1/2}. \quad (7)$$

A rigorous analysis would need to incorporate θ_τ and λ_s separately from θ_s and λ_s. However, for the sake of simplicity only one factor m is used. U^* is a normalized (modified) activation energy for twinning, and $\dot{\epsilon}_0$ is a reference parameter, and the exponent q varies between 4 and 8. Thus, the term

$$\left[\frac{U^*}{RT}\ln\frac{\dot{\epsilon}}{\dot{\epsilon}_0}\right]^{1/q}$$

shows a low temperature and strain-rate sensitivity. When the strain rate is increased from 10^{-2} to 10^3, this parameter changes by 10 to 60%.

The Hall–Petch slope for slip will not be discussed in the present paper. Let it suffice to state that:

$$\sigma_s = \sigma^* + k_s d^{-1/2} \quad (8)$$

σ^* represents the stress at which macro-slip occurs in monocrystals (temperature, strain and strain-rate sensitive) and should not be confused with σ_0, the frictional micro-yield stress in equation (6). Zerilli and Armstrong expressed σ_s in terms of thermally activated mechanisms for both f.c.c. [46] and b.c.c. [47] metals; for b.c.c. metals the σ_s takes the form:

$$\sigma_s = \sigma_s^* + C_2\,e^{-C_3 T}\dot{\epsilon}^{C_4 T} + k_s d^{-1/2}, \quad (9)$$

where σ_s^* is the athermal component of stress; C_2, C_3 and C_4 are material-dependent parameters. It has been demonstrated that the threshold stress for twinning is orientation dependent by De Angelis and Cohen [48]. These threshold pressures were experimentally determined by Murr [9] and correlated to the stacking-fault energy in f.c.c. metals. The orientation dependency will be ignored, as a first approximation. By setting $\sigma_s = \sigma_T$ it is possible to obtain the strain rate at which the slip-twinning transition is reached, at a prescribed temperature and strain rate; this is obtained by equations (7) and (9).

Under shock compression, the strain rates can be obtained through the phenomenological relationship obtained by Swegle and Grady [49, 50]. They measured shock-wave profiles for a number of materials and obtained the following relationship:

$$\dot{\epsilon} = k\sigma^4 \quad (10)$$

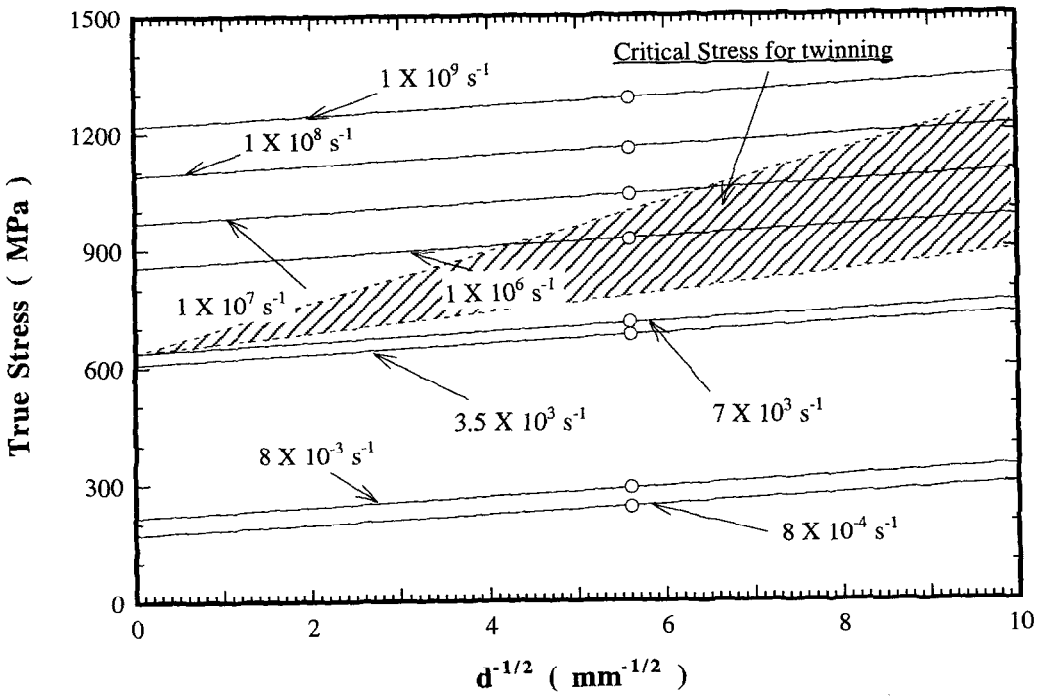

Fig. 13. Hall–Petch relation for slip (at different strain rates) and twinning (hatched area represents uncertainty).

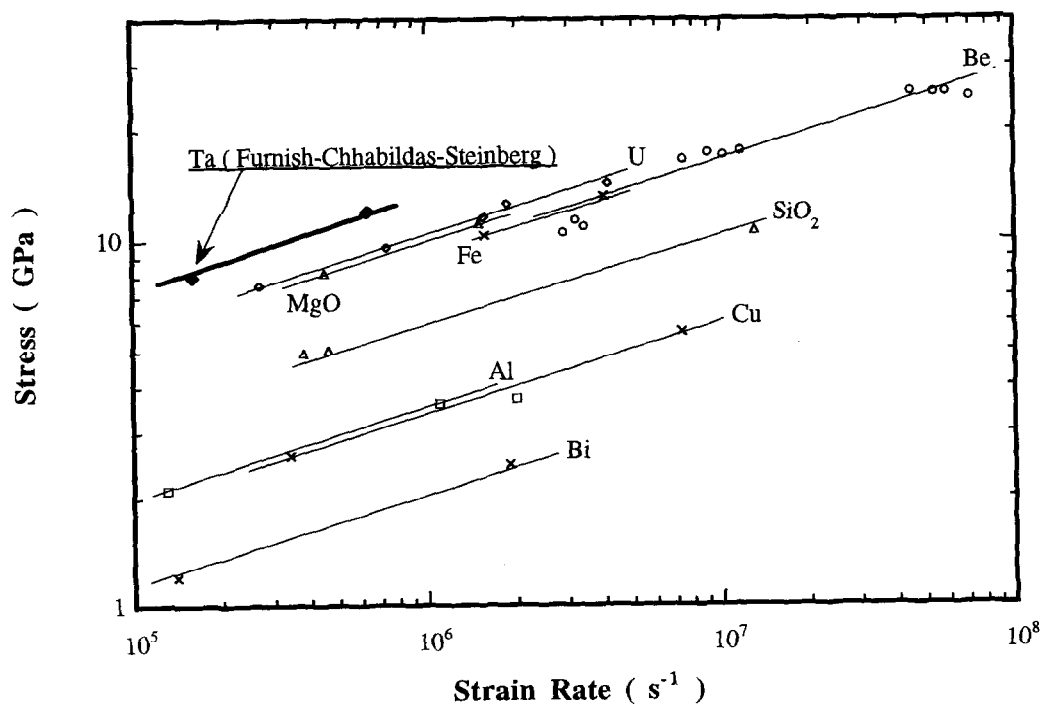

Fig. 14. Swegle—Grady [49, 50] plot relating peak stress and strain rate at the shock front; tantalum data added to plot [56, 57].

where k is material dependent. In equation (10), the stress is taken as the shock pressure. Through equations (7), (9) and (10) one arrives at:

$$\sigma = k^{-1/4}\left[\frac{\sigma_0 - \sigma_s^* + (k_T - k_s)d^{-1/2}}{C_2\, e^{-C_3 T}}\right]^{(4C_4 T)^{-1}}. \quad (11)$$

The application of the analysis above enables the prediction of the slip-twinning transition. The twinning stress for tantalum is not well established, and qualitative experiments such as the ones by Barrett and Bakish [11] do not provide quantitative values. The experimental observation of twinning in the mechanical testing of Ta monocrystals at 4.3 K by Mitchell and Spitzig [51] serves as a basis; it enables the determination of σ_0 (after conversion of shear into normal stresses). Mitchell and Spitzig [51] obtained twinning at 4.2 K when testing a [213] monocrystal. They report the value of the shear stress at which twinning occurs, along the slip system $[1\bar{1}1](011)$; this is the slip system, involving $[1\bar{1}1]$, which has the highest resolved shear stress. The slip direction $[1\bar{1}1]$ could be identified from Mitchell and Spitzig's [51] criterion:

$$h^2 + k^2 + l^2 < 4hl.$$

The corresponding tensile stress is:

$$\sigma_T = \frac{\tau_s}{\cos\theta_s \cos\lambda_s} = 900.5 \text{ MPa}.$$

In order to obtain the corresponding critical shear stress for twinning, one calculates the corresponding Schmid factor for the $(\bar{1}12)$ $[1\bar{1}1]$ twin direction and plane (the twin system reported by Mitchell and Spitzig [51]):

$$\cos\theta_T \cos\lambda_T = 0.332.$$

Thus $\tau_T = \sigma_0 \cos\theta_T \cos\lambda_T = 299.5$ MPa.

In order to obtain the corresponding normal stress for twinning, considering the texture observed in the specimens, the Schmid factors for all possible twinning systems were computed. The results are shown in Table 2, for [100] and [111] textures. For [100] texture, the maximum value of the Schmid factor is 0.471, yielding, correspondingly:

$$\sigma_0 = 635.9 \text{ MPa}.$$

For [111] texture, the corresponding normal stress σ_0 is equal to 953.8 MPa. Thus, the critical stress for twinning is higher. The Hall–Petch slope for twinning was taken as varying between 2 and 5 times k_s; this range is consistent with k_T/k_s ratios experimentally determined by Armstrong and Worthington [31], Armstrong and Zerilli [1], and Vöhringer [52]. The H–P slope for slip, which is given by Zerilli and Armstrong [47], falls in the range:

$$9 \leqslant k_s \leqslant 19 \text{ MPa mm}^{1/2}.$$

This yields, assuming $k_s = 12.9$ MPa mm$^{1/2}$, a value of:

$$25.8 \leqslant k_T \leqslant 64.5 \text{ MPa mm}^{1/2}.$$

For a grain size of 43 μm (specimens shock loaded in this investigation), the critical stress for twinning is found to be equal to (from equation (7)):

$$760.3 \leqslant \sigma_T \leqslant 946 \text{ MPa}.$$

The high-strain-rate yield stresses (by slip) for the material under investigation were obtained from the results of Meyers *et al.* [22] and are presented in Fig. 12, together with results by Hoge and Mukherjee [53]. The data are extrapolated to higher strain rates using a simple quadratic fit; the intersection of the twinning stress (a band was assumed because of uncertainty) with the extrapolated slip data provides the critical strain rate for twinning. Measurements were also made by Sherwood *et al.* [54] and Shields *et al.* [55]. Due to the uncertainties, it is in the 10^7–10^8 s^{-1} range. The data extrapolation ignores possible changes in dislocation motion controlling mechanisms (drag versus thermal/athermal barriers). Figure 13 shows the effect of grain size on the slip-twinning transition. The hatched band corresponds, again, to twinning, and the Hall–Petch slope of 12.9 MPa mm$^{1/2}$ was used to represent the grain-size dependence of flow stress by slip. For twinning, two slopes were used due to uncertainties. The results show very clearly that the slip-twinning transition occurs at a strain rate of $\sim 10^6$ s^{-1} for a monocrystal, whereas it requires a strain rate of 10^7–10^9 s^{-1} (uncertainty due to hatched region) for a grain size of 43 μm; these are the limits of the plot in Fig. 12. The correspondence between strain rate and shock stress was obtained through the Swegle–Grady relationship. Furnish *et al.* [56] and Steinberg [52] obtained shock-wave profiles for tantalum at pressures of 8 and 12 GPa. These profiles enabled the determination of strain rates which are plotted together with the data from Swegle and Grady [49, 50] in Fig. 14. The Swegle–Grady relationship is obeyed (equation (10)) and the coefficient k can be obtained: $k = 27.34$ s^{-1} (GPa)$^{-4}$. The application of equation (11) to tantalum, using the parameters C_2, C_3 and C_4 given by Zerilli and Armstrong [47], is shown in Fig. 15. The threshold stress for twinning (in shock loading) is plotted as a function of grain size for four different temperatures; 100, 200, 300 and 400 K. It should be noticed that this simple constitutive description does not incorporate a temperature correction for shock heating. This behaviour is consistent with the overall shock response of b.c.c. and f.c.c. metals and alloys, and therefore it is proposed that the constitutive description presented herein is not restricted to tantalum. The predictions of Fig. 15 are only in qualitative agreement with the experimental results: for the experiment described in this paper, the predicted transition pressure is 12 GPa. However,

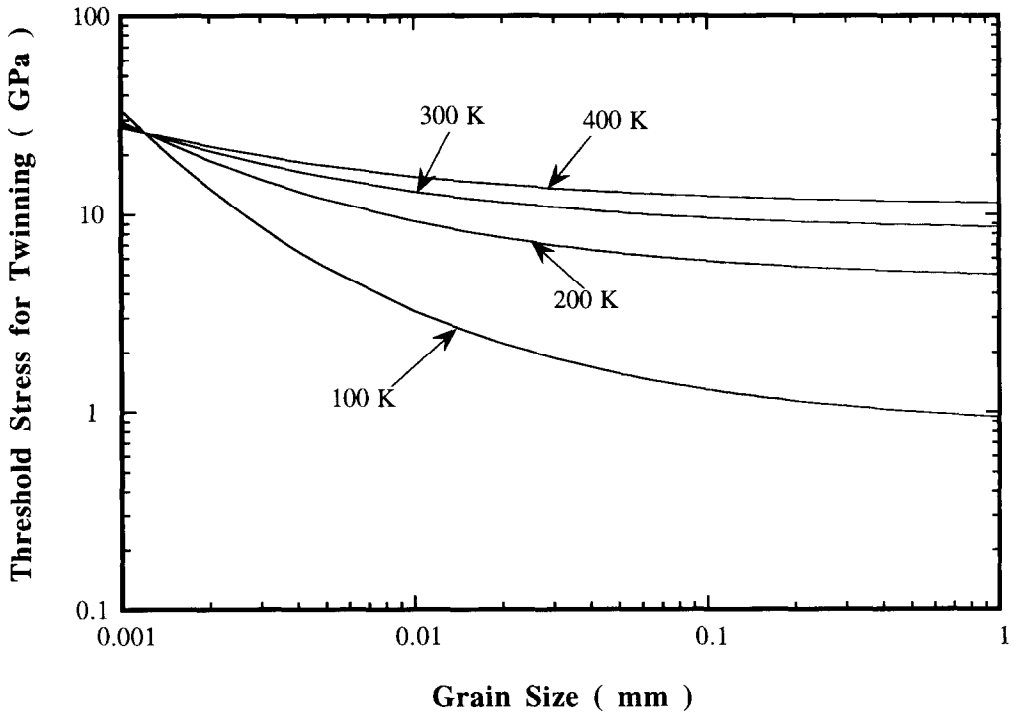

Fig. 15. Calculated shock threshold pressure versus grain size for different temperatures.

considering all the uncertainties in the data and constitutive description, the prediction is very satisfactory. The calculated threshold stress decreases with decreasing temperature and increasing grain size. At a grain size of 1.2 μm, the lines intersect, and for lower grain sizes the grain size dependency is inverted. It is not known, at present, whether this is a mathematical artefact; it might be pointed out that for twinning in shocked molybdenum, twin frequency irregularities also occurred in a range of small grain sizes (between 1 and 7 μm) [4].

4. CONCLUSIONS

Tantalum was subjected to shock compression at a pressure of 45 GPa and pulse duration of 1.8 μs in an explosively driven set-up. The microstructural changes included a high dislocation density and substantial mechanical twinning, which contributed to the enhanced hardening observed in post-shock mechanical testing (at both quasi-static and high strain rates). The twinning plane was identified as {112} and confirms earlier reports by Barrett and Bakish [11], Anderson and Bronisz [12], Jagannadham *et al.* [24] and Gray and Vecchio [15]. The post-shock flow stress of the material exceeds (by a value $\Delta\sigma \sim 50$–100 MPa) the flow stress of as-received material plastically deformed to a true strain of 0.22, equal to the effective transient shock strain. It is therefore concluded that mechanical twinning is responsible for the additional hardening of the microstructure.

A constitutive description of the twin-slip transition is proposed. It is based on the assumption of a very low temperature and strain rate dependence of the twinning stress, in accord with experimental results [1, 31, 32] and mechanistic predictions by Armstrong and Worthington [31] and Jagannadham *et al.* [24]. At a critical strain rate (temperature dependent) the flow curves for slip and twinning intersect, marking the initiation of the latter phenomenon. The shock pressure establishes the strain rate at the shock front through the Grady–Swegle [49, 50] relationship. This constitutive description yields quantitative predictions of the threshold stress for twinning in tantalum that are temperature and grain size dependent.

Acknowledgements—This research was supported by the US Army Research Office through Contracts No. DAAL03-92-G0108 (University Research Initiative Program on Dynamic Behavior of Ductile Materials) and No. DAAH04-94-G0314; and by the Dept. of US Army-ARDEC, Piccatiny Arsenal, NJ under Contract No. DAAA 21-94-C-0059. The shock loading of the specimen was carried out at the New Mexico Institute of Mining and Technology as a joint experiment with Dr D. Lassila, LLNL; his help through discussions and in machining of the set-up is gratefully acknowledged. The quasi-static experiments were carried out by Joy Hines and the dynamic experiments by Mr Jon Isaacs (CEAM). Their help is greatly appreciated. Discussions with Professors V. F. Nesterenko (UCSD), K. S. Vecchio (UCSD), J. Isaacs (UCSD) and R. W. Armstrong (University of Maryland) are gratefully acknowledged.

REFERENCES

1. R. W. Armstrong and F. J. Zerilli, *J. de Physique, Coll. C3* **49,** C3-259 (1980).
2. L. E. Murr, in *Shock Waves and High-Strain Rate Phenomena in Metals*, p. 607, (edited by M. A. Meyers and L. E. Murr), Plenum, New York (1981).
3. G. E. Dieter, in *Response of Metals to High Velocity Deformation*, p. 409, Wiley Interscience, New York (1961).
4. K. Wongwiwat and L. E. Murr, *Mater. Sci. Eng.* **35,** 273 (1978).
5. G. T. Gray, III in *High Pressure Shock Compression of Solids*, p. 187, (edited by J. R. Asay and M. Shahinpoor), Springer-Verlag, New York (1993).
6. R. Asfhani, E. Chen and A. Crowson (Eds.), *High Strain Rate Behavior of Refractory Metals and Alloys*, The Metallurgical Society, Warrendale, PA (1992).
7. M. A. Meyers, L. E. Murr and K. P. Staudhammer (Eds.), in *Shock Wave and High-Strain-Rate Phenomena in Materials*, Marcel Dekker, New York (1992).
8. M. A. Meyers and L. E. Murr, in *Shock Waves and High-Strain-Rate Phenomena in Metals*, p. 487, (edited by M. A. Meyers and L. E. Murr), Plenum, New York (1981).
9. L. E. Murr, in *Shock Waves in Condensed Matter*, p. 315, (edited by S. C. Schmidt and N. C. Holmes). Elsevier, Amsterdam (1988).
10. R. C. Koo, *J. Less Common Metals* **4,** 138 (1962).
11. C. S. Barrett and R. Bakish, *Trans. AIME* **212,** 122 (1958).
12. L. W. Anderson and S. E. Bronisz, *Acta metall.* **7,** 645 (1959).
13. T. K. Chatterjee and C. Feng, in *Proc. 45th Annual Meeting of the Electron Microscopy Soc. of America*, p. 234, (edited by W. Bailey), San Francisco Press, San Francisco (1987).
14. C. L. Wittman, R. K. Garrett, Jr., J. B. Clark and C. M. Lopatin, in *Shock-Wave and High-Strain-Rate Phenomena in Materials*, p. 925, (edited by M. A. Meyers, L. E. Murr and K. P. Staudhammer), Marcel Dekker, New York.
15. G. T. Gray III and K. S. Vecchio, *Metall. and Mater. Trans.* **26A,** 2555 (1995).
16. A. J. Strutt, K. S. Vecchio, S. R. Bingert and G. T. Gray III, Effect on interstitials on the mechanical behavior of P/M tantalum, in *Tungsten and Refractory Metals*, **3,** M PIF, Princeton, NJ (1995).
17. F. Sandstrom, Private communication, CETR report, New Mexico Institute of Mining and Technology, Socorro, NM.
18. M. A. Mogilevsky and L. A. Teplyakova, in *Metallurgical Applications of Shock-Wave and High-Strain-Rate Phenomena*, p. 419, (edited by L. E. Murr, K. P. Staudhammer and M. A. Meyers), Marcel Dekker, New York (1986).
19. G. T. Gray III, P. S. Follansbee and C. E. Frantz, *Mat. Sci. Eng.* **A111,** 9 (1989).
20. G. T. Gray III, in *Shock Compression of Condensed Matter—1989*, p. 407, (edited by S. C. Schmidt, J. N. Johnson and L. W. Davison), North-Holland, Amsterdam (1990).
21. R. G. McQueen, S. P. Marsh, J. W. Taylor, J. N. Fritz and W. J. Carter, in *High-Velocity Impact Phenomena*, p. 293, Appendix E, (edited by R. Kinslow), Academic Press, New York (1970).
22. M. A. Meyers, Y.-J. Chen, F. D. S. Marquis and D. S. Kim, *Met. and Mat. Trans.* **26A,** 2493 (1995).
23. L. E. Murr, *Electron and Ion Microscopy and Microanalyses: Principles and Applications*, 2nd Edition, Marcel Dekker, New York (1992).
24. K. Jagannadham, R. W. Armstrong and J. P. Hirth, *Phil. Mag. A* **68,** 419 (1993).
25. R. Bullough and C. M. Wayman, *Trans. AIME* **236,** 1704 (1966).
26. C. M. Wayman and R. Bullough, *Trans. AIME* **236,** 1710 (1966).
27. M. A. Meyers, *Dynamic Behavior of Materials*, p. 388, Wiley, New York (1994).
28. C. L. Wittman, C. L. Lopatin, J. P. Swensen and T. J. Holmquist, in *High Strain Rate Behavior of Refractory Metals and Alloys*, p. 167, (edited by R. Ashfani, E. Chen and A. Crowson), The Metallurgical Society, Warrendale, PA (1992).
29. S. Nemat-Nasser, Y.-F. Li and J. B. Isaacs, *Mech. of Matls.* **17,** 111 (1994).
30. M. A. Meyers, U. R. Andrade and A. H. Chokshi, *Met. and Mat. Trans.* **26A,** 2881 (1995).
31. R. W. Armstrong and P. J. Worthington, in *Metallurgical Effects at High Strain Rates*, p. 401, (edited by R. W. Rohde, B. M. Butcher, J. R. Holland and C. H. Karnes), Plenum, New York (1973).
32. S. G. Song and G. T. Gray III, *Met. and Mat. Trans.* **26A,** 2665 (1995).
33. D. Hull, *Acta metall.* **9,** 191 (1961).
34. P. J. Worthington and E. Smith, *Acta metall.* **14,** 35 (1966).
35. V. F. Moisev and V. I. Trefilov, *Phys. Stat. Sol.* **18,** 881 (1966).
36. M. J. Marcinkowski and H. A. Lipsitt, *Acta metall.* **10,** 95 (1962).
37. W. S. Owen and D. Hull, in *Refractory Metals and Alloys: II*, p. 1, (edited by M. Semchyshen and I. Perimutter), Interscience, New York (1963).
38. D. Löhe and O. Vöhringer, *Z. Metallkunde* **77,** 557 (1980).
39. O. Vöhringer, *Metall.* **12,** 1150 (1976).
40. R. W. Armstrong, in *Advances in Materials Research*, p. 101, vol. 5, (edited by R. F. Bunshah), Wiley, New York (1971).
41. E. O. Hall, *Proc. Roy. Soc. (London)* **B64,** 474 (1951).
42. N. J. Petch, *J. Iron Steel Inst.* **174,** 25 (1953).
43. A. H. Cottrell, *Trans. TMS-AIME* **212,** 192 (1958).
44. L. E. Murr and S. S. Hecker, *Scripta metall.* **13,** 167 (1979).
45. M. A. Meyers and E. Ashworth, *Phil. Mag.* **46,** 737 (1982).
46. F. J. Zerilli and R. W. Armstrong, *J. Appl. Phys.* **61,** 1816 (1987).
47. F. J. Zerilli and R. W. Armstrong, *J. Appl. Phys.* **68,** 1580 (1990).
48. R. J. De Angelis and J. B. Cohen, *J. of Metals* **15,** 681 (1963).
49. J. W. Swegle and D. E. Grady, *J. Appl. Phys.* **58,** 692 (1985).
50. J. W. Swegle and D. E. Grady, in *Shock Waves in Condensed Matter—1985*, p. 353, (edited by Y. M. Gupta), Plenum, New York (1986).
51. T. E. Mitchell and W. A. Spitzig, *Acta metall.* **13,** 1169 (1965).
52. O. Vöhringer, *Z. Metallkunde* **67,** 518 (1976).
53. K. G. Hoge and A. K. Mukherjee, *J. Mat. Sci.*, **12,** 1666 (1977).
54. P. J. Sherwood, F. Guiu, H. C. Kim and P. L. Pratt, *Can. J. of Physics* **45,** 1075 (1967).
55. L. A. Shields, S. H. Goods, R. Gibala and T. E. Mitchell, *Matls. Sci. and Eng.* **20,** 71 (1975).
56. M. D. Furnish, L. C. Chhabildas and D. J. Steinberg, in *High Pressure Science and Technology—1993*, p. 1099, APS (1994).
57. D. J. Steinberg, Modeling release behavior in shocked tantalum, in *Shock Waves* in *Condensed Matter—1995*, APS, in press.